#### Research Article

Cao Jun, Wu Zheshu, Cui Zhen\*, and Mei Xiancheng

# Mechanical testing and engineering applicability analysis of SAP concrete used in buffer layer design for tunnels in active fault zones

https://doi.org/10.1515/rams-2024-0002 received October 23, 2023; accepted February 27, 2024

Abstract: To tackle the challenge of dislocation damage when tunnels traverse active fault zones, this study introduces the concept of using brittle buffer materials for antidislocation. Building on this concept, we propose a novel concrete buffer material utilizing large-sized spherical super absorbent polymers (SAP) as a porogen, aimed at ensuring the safety of tunnel structures during active fault dislocations. To investigate the feasibility and superiority of SAP concrete as a buffer material compared to other similar materials, we prepared samples with three different SAP concrete proportions and conducted a series of physical and mechanical tests. The results show that SAP pre-hydrated with 0.2 mol·L<sup>-1</sup> sodium carbonate solution exhibits a slower rate of moisture loss in the cement slurry, aiding the hydration reaction of concrete. The permeability coefficient of SAP concrete is approximately  $10^{-7}$  cm·s<sup>-1</sup>, slightly lower than foam concrete of the same density level. SAP concrete buffer material demonstrates significant brittleness, in contrast to the mostly ductile nature of other buffers such as foam concrete and rubberized concrete. Utilizing the brittle nature of SAP concrete materials, when applied to tunnels affected by stick-slip active fault dislocations, its instantaneous loss of compressive capacity provides excellent yield performance, thus protecting the tunnel lining from damage. However, under certain circumferential pressure conditions, both the

peak and residual strength of SAP concrete significantly increase. High peak and residual strengths do not favor the effective buffering effect of SAP concrete; therefore, an approach involving the intermittent arrangement of precast buffer blocks has been proposed for application.

**Keywords:** SAP concrete, buffer material, anti-dislocation, tunnel

#### **Nomenclature**

SAP super absorbent polymer
EPS expandable polystyrene
K permeability coefficient
Q measured flow

L height of soil sample passing through seepage

A fractal dimension H measured head loss  $\tau$  shear strength

 $\sigma$  normal compressive stress on shear damage

surface cohesion

 $\phi$  angle of internal friction

### 1 Introduction

When constructing a tunnel in a fault zone area, it is inevitable to cross the active fault zone. When the active fault is misaligned, especially after adhesive slip fracture, it often causes severe compression, tension, and shear damage to the lining, seriously affecting the tunnel function and threatening the safety of the tunnel [1–8]. The Kobe earthquake in 1995 [1], the Türkiye earthquake in 1999 [2–4], the Chi-Chi earthquake in 1999 [5–7], the Wenchuan earthquake in 2008 [8], and the Menyuan earthquake in 2021 [9] have proved this point. The dislocation and fracture damage that occurred in the Daliang Tunnel during the

Geotechnical Engineering, Institute of Rock and Soil Mechanics, Chinese Academy of Sciences, Wuhan, Hubei 430071, China; School of Engineering Science, University of Chinese Academy of Sciences, Beijing, 10049, China

**Wu Zheshu:** China Railway Siyuan Survey and Design Group Co., Ltd., Wuhan, Hubei, 430063, China

<sup>\*</sup> Corresponding author: Cui Zhen, State Key Laboratory of Geomechanics and Geotechnical Engineering, Institute of Rock and Soil Mechanics, Chinese Academy of Sciences, Wuhan, Hubei 430071, China; School of Engineering Science, University of Chinese Academy of Sciences, Beijing, 10049, China, e-mail: zcui@whrsm.ac.cn Cao Jun, Mei Xiancheng: State Key Laboratory of Geomechanics and Geotechnical Engineering, Institute of Rock and Soil Mechanics, Chinese



Figure 1: Damages caused by faults in the Daliang Tunnel.

Menyuan earthquake was especially typical, as shown in Figure 1. Therefore, how to reduce tunnel structural damage caused by fault displacement has become a key issue that needs to be overcome urgently.

The utilization of flexible connections is a commonly employed strategy for resisting tunnel dislocations, capable of significantly reducing the strain on the lining structure [10-12]. However, vertical displacements occurring between hinge joints can induce abrupt changes in the elevation of the tunnel surface, leading to a serrated morphology of the lining. Such alterations may result in structural damage to the original pavement, thereby complicating post-event maintenance. Additionally, numerous scholars have discussed the implementation of a buffer layer, which serves to absorb energy and relieve pressure, as depicted in Figure 2. Nevertheless, the buffer materials predominantly in use today are ductile, such as foam [13-18] and flexible damping materials [19-21]. These materials exhibit several limitations in application: (1) during the preparation process, if the slurry consistency of foam

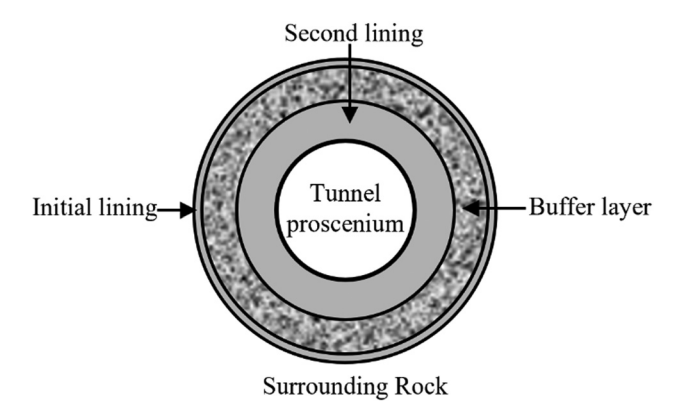


Figure 2: Sketch map of buffer layer yielding support in tunnel.

concrete is too low, it may fail to encapsulate the gases produced by the foaming agent, leading to gas escape and subsequent foam collapse [22–24]; expandable polystyrene (EPS) concrete tends to rise and segregate significantly during preparation due to the low density of EPS [25,26]. (2) Most existing buffer materials, being ductile, continue to transmit fault dislocation loads to the tunnel's secondary lining upon entering the plastic state, thereby increasing the likelihood of damage to the secondary lining.

In consideration of the aforementioned issues, a method utilizing brittle buffer materials for resisting fault dislocation is proposed, and the properties of this brittle material are defined as follows: (1) the material should have a uniform distribution of internal cavities: (2) the material should possess an appropriate compressive strength. Based on preliminary calculations and engineering experience, the compressive strength is determined to be 1-6 MPa [16]; and (3) when subjected to fault dislocation loads, the buffer material should exhibit brittle failure characteristics after reaching its peak strength, thus rapidly creating space and ensuring that the load imposed on the secondary lining is minimized as much as possible. Consequently, this article primarily aims to introduce a novel type of honeycomb concrete buffer material, utilizing super absorbent polymers (SAP) as pyrogens, in accordance with the aforementioned specifications.

The proposed concept of using brittle buffer materials to resist fault dislocation, as illustrated in Figure 3, involves excavating and filling with brittle buffer materials near the fault zone. The excavation depth is determined by the maximum fault displacement and is typically not less than half of this displacement. The fracturing of the brittle materials provides deformation space for the surrounding rock, thereby mitigating and dispersing the localized shear damage to the lining at the fault location.

SAP is a quintessential type of functional polymer material. They are capable of absorbing and retaining several hundred to even thousands of times their own weight in water, leading to significant volume expansion [27,28], and they exhibit a certain degree of water retention capacity. Based on the volumetric expansion and water-retention characteristics of hydrated SAP, current research in the concrete sector is divided into two main categories: (1) studies on the "internal curing" of concrete utilizing SAP's water-holding properties [29-30] and (2) research on the fabrication of honeycomb concrete. Given the volumetric expansion upon hydration, using water-saturated SAP as an aggregate in concrete allows for the creation of internal cavities when the SAP dehydrates and contracts, thereby yielding honeycomb concrete with controllable pore shapes and sizes [31]. The hydrated SAP has substantial support

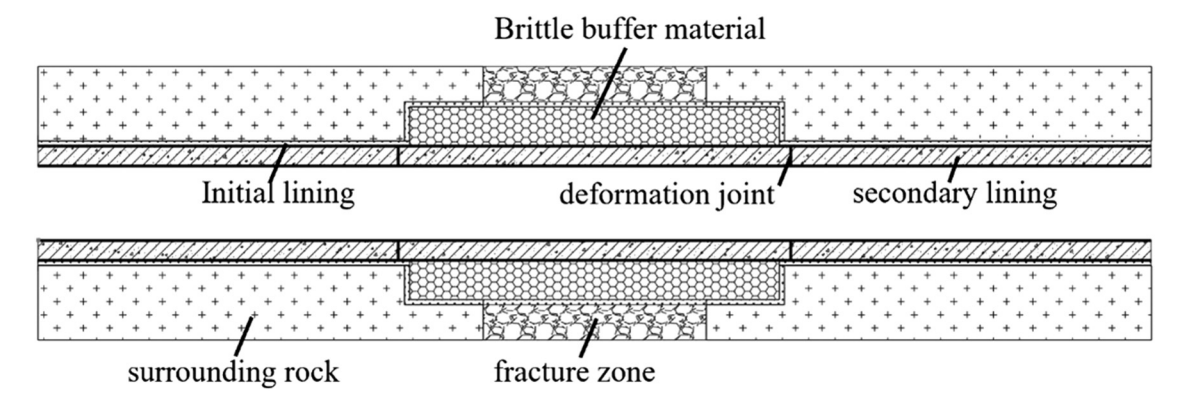


Figure 3: Diagram of brittle cushioning concept to resist misfiring.

capacity and increased density, which can prevent issues such as collapse or lavering encountered with materials like foam concrete and EPS concrete. Additionally, by controlling the diameter, gradation of different SAP aggregates, and the grade of cement, brittle buffer materials with varying strengths and mechanical properties can be manufactured.

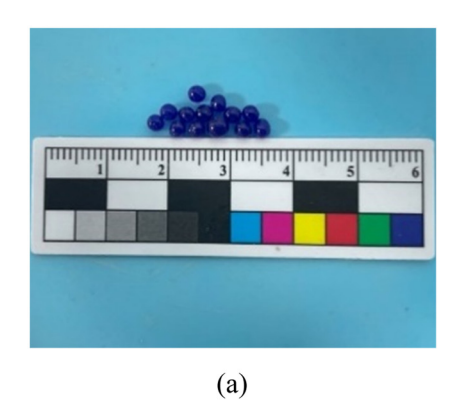
Until now, there have been limited studies on the fabrication of honeycomb concrete using large-diameter SAP as a pore-forming agent. Deng et al. [32] investigated the compression behavior of millimeter-scale SAP honeycomb concrete and established the relationships between porosity, strain rate, and mechanical properties such as compressive strength, splitting tensile strength, flexural strength, and elastic modulus. Ren [33] conducted Split Hopkinson Pressure Bar tests on SAP concrete based on ABAOUS, revealing the variation in lateral confinement effects with strain rate or porosity. Based on research into the internal pore structure of functional concrete using SAP as a porogen, Wang et al. [34] found that the addition of spherical SAP could delay the reduction of internal relative humidity in concrete and significantly reduce its mechanical properties. Furthermore, through analysis, they obtained the water absorption and release rates of SAP in solutions of different concentrations.

Building on prior studies, this article endeavors to produce honevcomb concrete (hereafter referred to as SAP concrete) utilizing large-diameter spherical SAP as a pore-forming agent, aimed at functioning as a brittle buffer material for tunnel anti-dislocation. Initially, the preparation method of SAP concrete is meticulously described, followed by a discussion of its physical and mechanical properties. Subsequently, the viability of this material as an ideal buffer for tunnel anti-dislocation is validated.

### 2 Water absorption and water loss characteristics of large-diameter SAP aggregate

#### 2.1 Water absorption of SAP aggregate

The SAP utilized had a pre-soaking particle size of approximately 2-3 mm. The SAP was pre-hydrated using both distilled water and a 0.2 mol·L<sup>-1</sup> sodium carbonate solution, as shown in Figure 4. At different times during the soaking



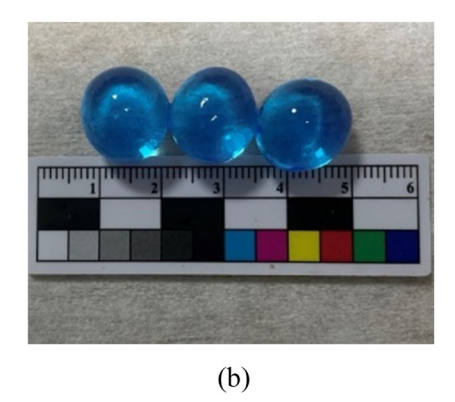
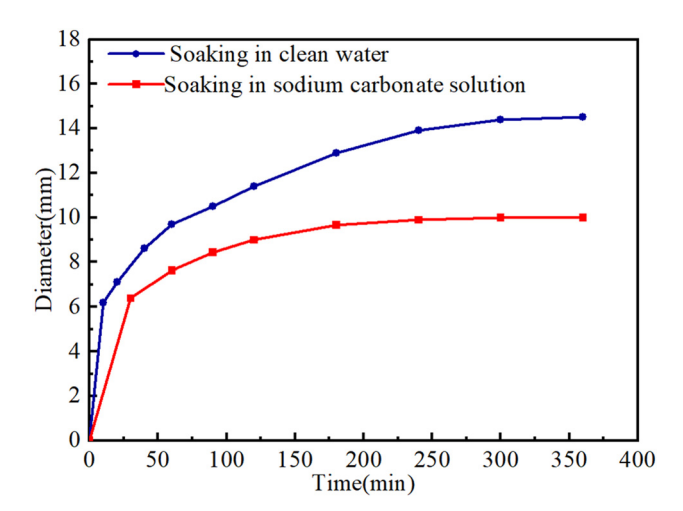


Figure 4: Comparison of SAP aggregates before and after absorbing water: (a) before absorbing water and (b) after absorbing water.



**Figure 5:** Water absorption process of SAP aggregates in different solutions.

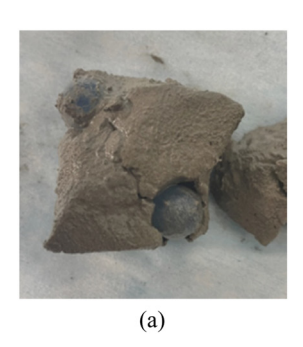
process, the SAP was retrieved to measure its dimensions, and the trend of its size change over time was plotted, as illustrated in Figure 5. It is evident that the SAP can reach a saturated state after 8 h of soaking in either distilled water or a  $0.2\,\mathrm{mol}\cdot\mathrm{L}^{-1}$  sodium carbonate solution. The diameter upon saturation in distilled water is 15 mm, while it is approximately 10 mm when saturated in a  $0.2\,\mathrm{mol}\cdot\mathrm{L}^{-1}$  sodium carbonate solution.

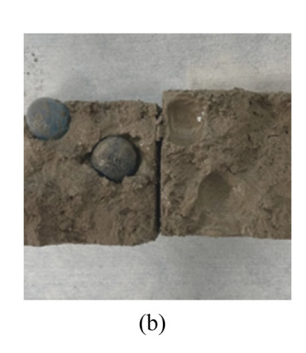
### 2.2 Water loss characteristics of saturated SAP aggregates in cement slurry

SAP saturated in different solutions was incorporated into a cement slurry with a water-to-cement ratio of 0.3. The SAP was extracted at various intervals to measure its dimensions and track the trend of moisture loss, as depicted in Figures 6 and 7. The moisture loss curve of SAP in the cement slurry was plotted, as shown in Figure 8. It is evident that the moisture loss of SAP pre-treated with distilled water primarily occurs

within the first 2 h. Observing the cavities in the specimens cut at different times, it is clear that significant moisture accumulation is present within the cavities for the first 60 min, with SAP extensively contacting the cavity walls. After 60 min, the amount of moisture in the cavities noticeably reduces, and the SAP separates from the cavity walls. The moisture loss process of SAP pre-treated with distilled water in the cement slurry can be divided into the following two stages: (1) moisture loss due to the osmotic pressure difference between the SAP and the solution in the cement slurry and (2) dehydration of SAP in the cavities due to the humidity difference within the cavity post-formation. The first stage primarily occurs within the first 60 min after pouring, while the second stage predominantly takes place after 60 min. It was discovered that due to the significant difference in ion concentration, SAP soaked in distilled water rapidly loses a substantial amount of water, leading to an increase in the water-to-cement ratio. This phenomenon can easily cause segregation in SAP concrete, diminish the strength of SAP concrete, and exacerbate the degree of stratification. Compared to SAP soaked in distilled water (Figure 5), SAP immersed in an alkaline solution exhibits almost no size change initially, with slow moisture loss starting after 4 h, and subsequent moisture loss occurring very gradually. This is because the SAP pre-treated with an alkaline solution can achieve osmotic pressure equilibrium with the cement slurry. In the early stages, it does not only lose water due to osmotic pressure but only experiences moisture loss later on due to humidity differences. This avoids the segregation and stratification issues caused by the rapid water loss of SAP leading to an increased waterto-cement ratio.

Although SAP pre-treated with an alkaline solution has a smaller size after soaking, its dehydration process in the cement slurry is slow, effectively preventing the occurrence of segregation and bleeding in the cement slurry. Therefore, subsequent work will adopt the approach of soaking SAP aggregates in an alkaline solution to reduce the rate of water loss of SAP in cementitious materials. The







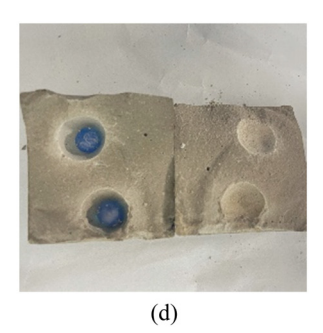
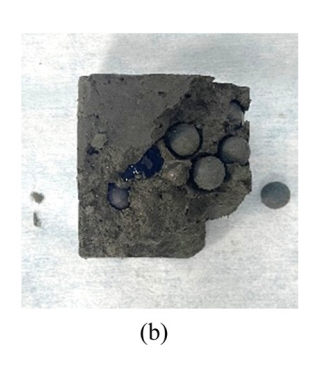
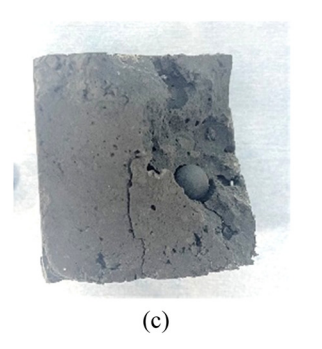


Figure 6: Dewatering process in specimens of SAP aggregates saturated in clear water: (a) 30 min, (b) 1 h, (c) 16 h, and (d) 1 day.







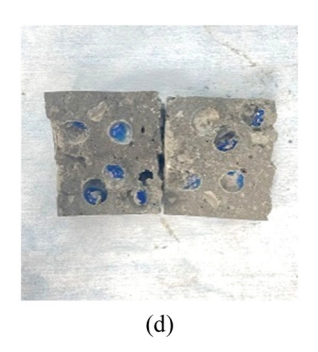
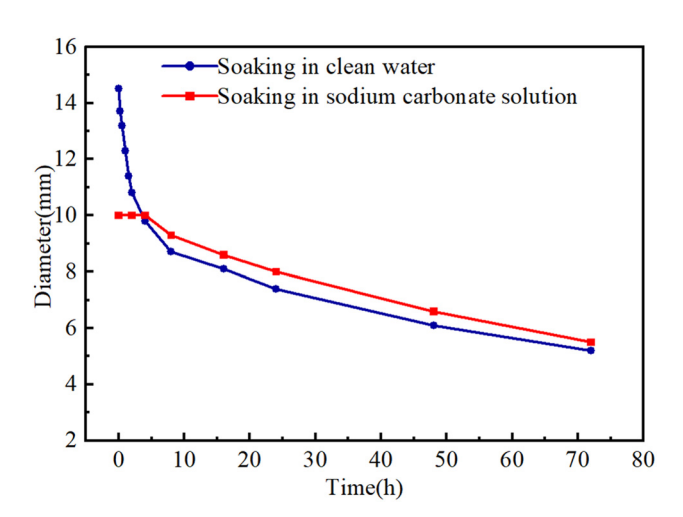


Figure 7: Dewatering process in specimens of SAP aggregates saturated in sodium carbonate solution. (a) 1 h, (b) 16 h, (c) 1 day, and (d) 3 days.



**Figure 8:** Dewatering process in cement slurry of saturated SAP aggregates with different pretreatments.

final method for pre-treating the SAP aggregates has been determined to be soaking in a 0.2 mol·L<sup>-1</sup> sodium carbonate solution for over 10 h.

# 3 Preparation of buffer material made of SAP aggregates

#### 3.1 Raw materials

In the preparation of SAP concrete, the raw materials utilized include P.O. 42.5 cement and sand with a particle size of less than 1 mm. The chosen SAP, as described in the previous section, was pre-hydrated using a  $0.2\,\mathrm{mol}\cdot\mathrm{L}^{-1}$  sodium carbonate solution. The composition of the composite admixture includes polycarboxylate superplasticizer and hydroxypropyl methylcellulose (HPMC) with a viscosity of 200,000.

#### 3.2 Mixing proportion

Materials with low density and strength typically exhibit relatively good buffering effects [35]. The higher the strength of the buffer layer, the greater the corresponding stress exerted on the secondary lining. Therefore, under the condition of ensuring the normal load-bearing capacity of the tunnel, buffer materials with lower strength should be selected as much as possible. To meet the basic performance requirements of buffer materials, this study selected three different mix proportion schemes for research. These proportions have moderate strength and cover a certain range of strength levels. The experimental grouping is shown in Table 1.

The dosages of polycarboxylate superplasticizer and HPMC were determined to be 0.3% and 0.2% of the cement, respectively, to adjust the consistency of the cement mortar, with a water-to-cement ratio of 0.3. Standard cubic specimens of 150 mm  $\times$  150 mm and standard cylindrical specimens of 50 mm  $\times$  100 mm were prepared.

#### 3.3 Preparation procedures

Initially, spherical SAP is pre-soaked as described in Section 2.1 to achieve a saturated state. SAP concrete is then prepared according to the designed proportions. All dry

Table 1: Test group

Group no.	Sand–cement ratio	Volume fraction of saturated SAP aggregate (%)	Diameter of saturated SAP (mm)
S1	0.5	40	9
S2	0.3	50	9
S3	0.5	50	9

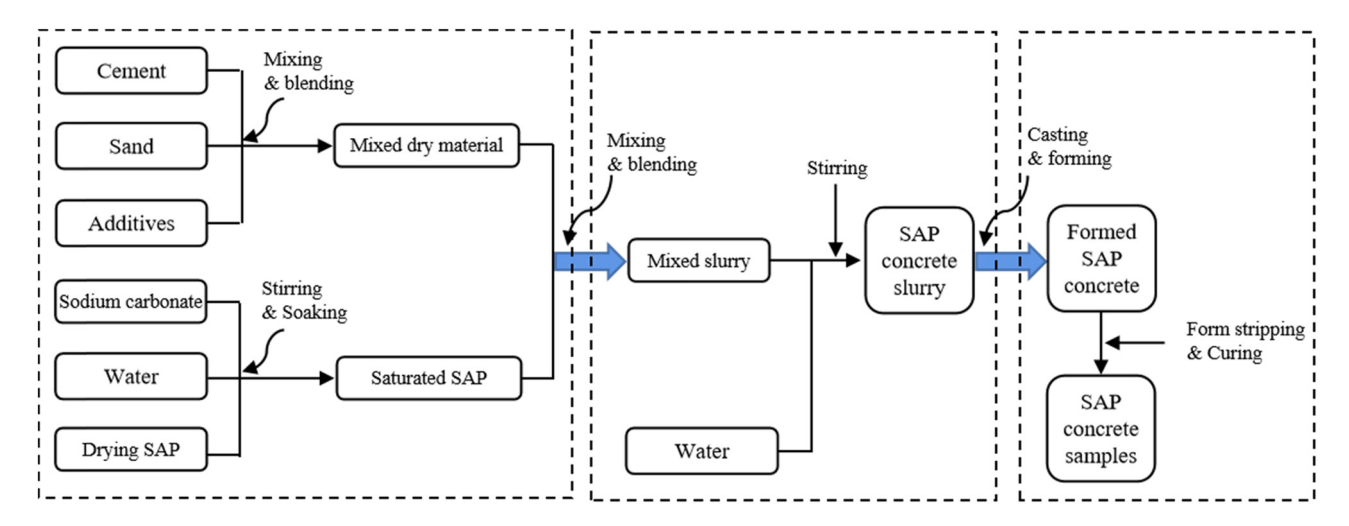


Figure 9: Preparation process of SAP concrete.

materials are mixed first, followed by the addition of the required amount of water and SAP, ensuring even blending. The well-mixed slurry is poured into molds and vibrated for 30 s. After the slurry solidifies for 24 h, the specimens are demolded and then placed in a standard curing box for 28 days of curing. The preparation process is shown in Figure 9.

# 4 Physical properties of SAP concrete buffering material

#### 4.1 Analysis of cavitation segregation

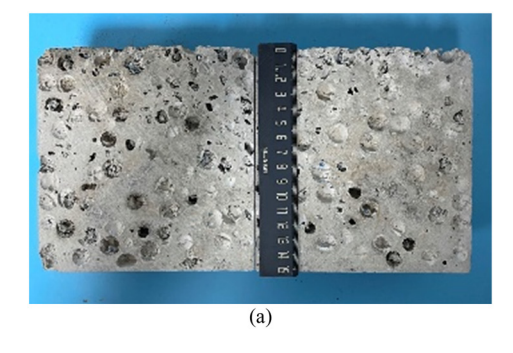
As a buffer material for tunnel anti-dislocation, SAP concrete should possess good characteristics of uniform spatial distribution of cavities. To this end, the cavity distribution of the prepared SAP concrete was investigated. Figure 10 shows a test section to visualize the cavity distribution pattern in SAP concrete. To further study the uniformity of internal cavity

distribution in SAP concrete buffer material, Figure 11 displays a computed tomography (CT) scan image showing the cavity distribution of SAP concrete buffer material using industrial CT scanning. It is evident that SAP is randomly distributed within the concrete, with no apparent settling or floating.

To investigate whether the large-size components still meet the required requirements for uniformity, large-size specimens with dimensions of 500 mm × 500 mm × 500 mm were prepared and sampled, as shown in Figure 12 and mechanical properties at the different positions were analyzed to verify their uniformity. Figure 13 shows the distribution of density and strength of SAP concrete components in different positions. As the difference in density and strength between different positions is small, so it can be considered that the uniformity of SAP concrete components is good.

#### 4.2 Microscopic properties

After curing for 28 days, the specimens were dried and then observed using a scanning electron microscope



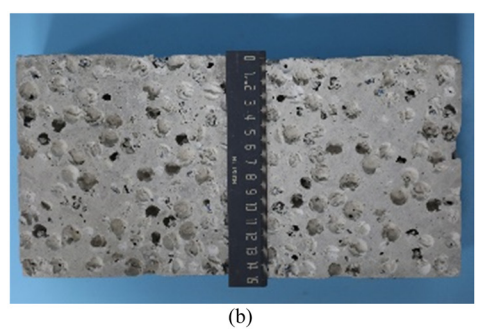
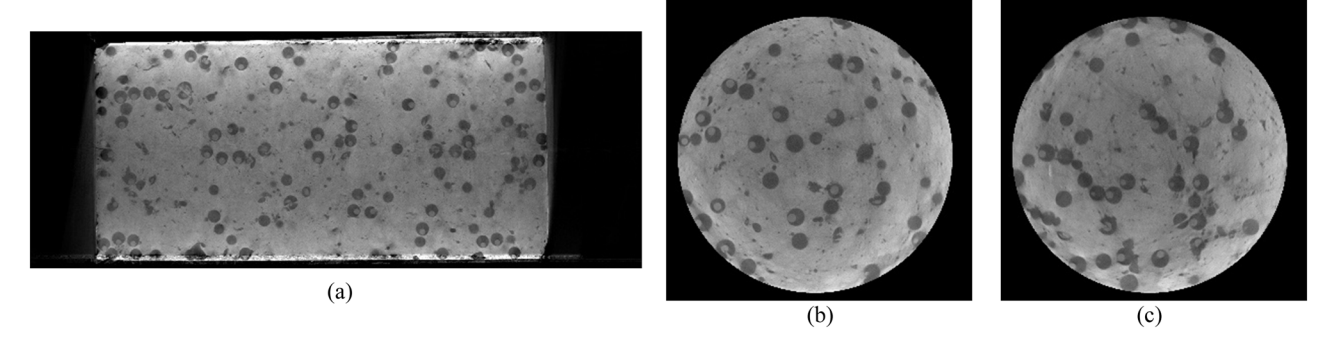


Figure 10: Cut sections of SAP concrete specimens. (a) Volume fraction of 40% SAP. (b) Volume fraction of 50% SAP.



**Figure 11:** CT scanning image of SAP concrete specimens. (a) Longitudinal section of cylindrical specimen. (b) Transverse section of cylindrical specimen 1. (c) Transverse section of cylindrical specimen 2.

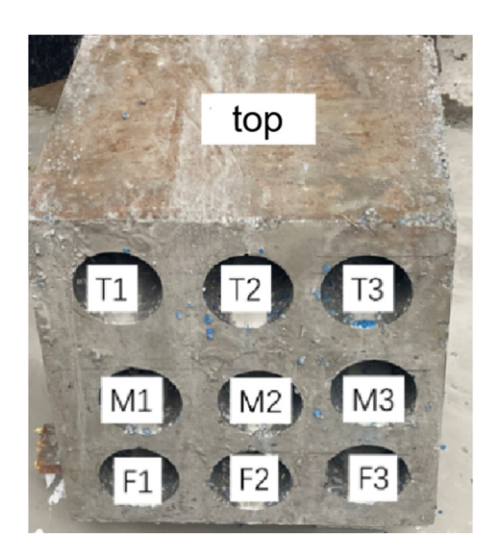


Figure 12: Sampling locations in large components.

(SEM) to examine the cavities and their surrounding microfeatures. Photographs were taken of the wall surfaces and the extreme transition zones of the cavities. The results, as shown in Figure 14, indicate that the moisture release from SAP had a certain impact on the interfacial transition zone, generating a large number of needle-like crystalline substances (ettringite) on the surface of the cavity walls. The ettringite forms elongated, branch-like crystal structures, interlacing like fibers, which to some extent inhibits cracking in the cementitious matrix.

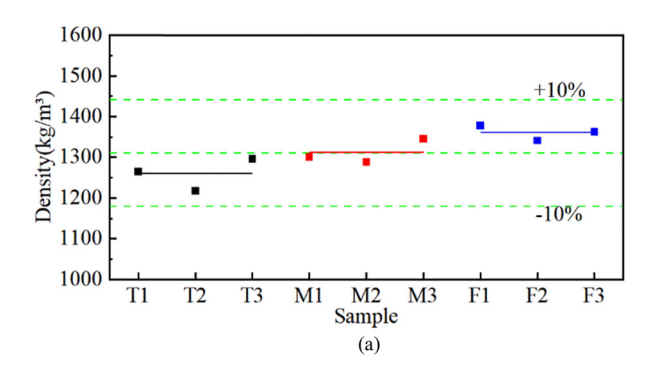
#### 4.3 Permeability resistance

Given that SAP concrete is porous, it may exhibit a certain degree of permeability. A permeability test was designed to investigate the permeability of SAP concrete. The test was conducted using a flexible wall permeameter, as shown in Figures 15 and 16, applying a confining pressure of 0.08 MPa and a permeation pressure of 0.06 MPa to measure the quantity of permeated water for calculating the permeability coefficient.

The permeability coefficient is calculated according to Darcy's law using the following formula:

$$K = \frac{QL}{AH},\tag{1}$$

where Q is the measured flow rate (m<sup>3</sup>·s<sup>-1</sup>), A is the cross-sectional area of the specimen (m<sup>2</sup>), L is the height of the



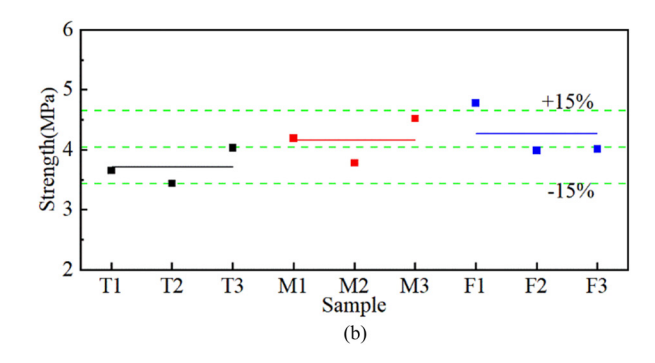


**Figure 13:** Distribution of density and strength of SAP concrete in large-size specimens. (a) Density distribution of SAP concrete component. (b) Compressive strength distribution of SAP concrete components.

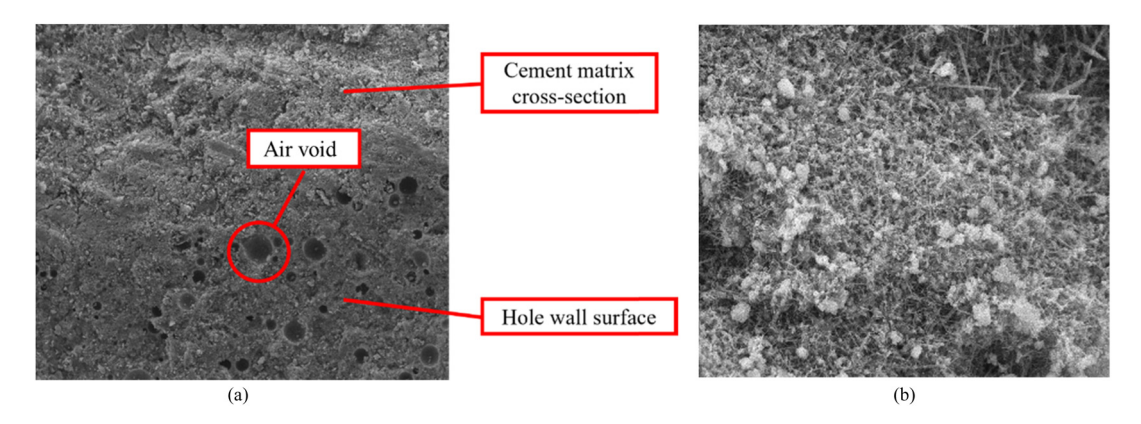


Figure 14: Microscopic morphology of SAP concrete (SEM). (a) Cavitation transition zone formed in SAP (200:1). (b) Cavitation surface of SAP (2,000:1).

specimen (m), and H is the measured hydraulic head loss (m). The calculated results are shown in Table 2.

The permeability coefficients of the above proportioned SAP concrete materials were measured to be of the order of  $10^{-7} \, \text{cm} \cdot \text{s}^{-1}$ , while the permeability coefficient of foam concrete is generally between the order of  $10^{-6}$  and  $10^{-7} \, \text{cm} \cdot \text{s}^{-1}$ , indicating that the permeability resistance of SAP concrete is slightly better than that of foam concrete.

Table 3. Figure 17 displays the uniaxial stress-strain curves and the test results of the mechanical parameters of the SAP concrete. Under uniaxial stress, SAP concrete exhibited a brittle failure mode with distinct splitting cracks. The stress–strain curve rapidly declined after reaching the peak strength, and the specimens collapsed under pressure. After collapse, due to the friction between the fragments, a certain stable residual strength was maintained.

### 5 Mechanical properties of SAP concrete buffer materials

#### 5.1 Uniaxial mechanical properties

To investigate the mechanical properties of SAP concrete, uniaxial compression tests were conducted on each group of SAP concrete listed in Table 1, with results presented in



Figure 15: Soft wall permeameter.



Figure 16: Saturated specimens.

Table 2: Permeability coefficients of SAP concrete materials

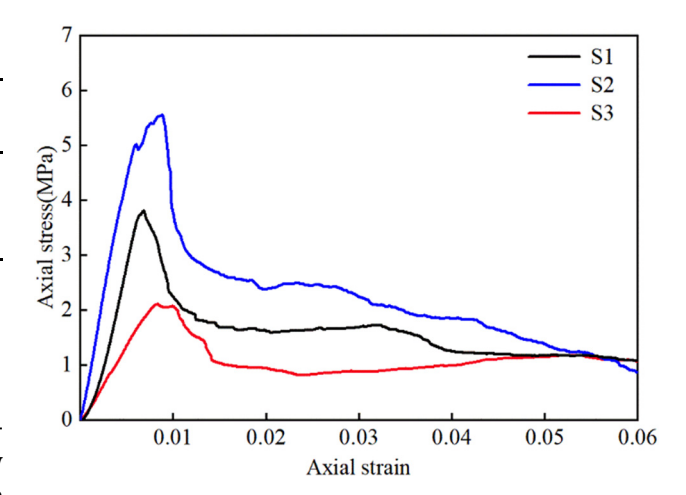
No.	Dry density (g∙cm <sup>−3</sup> )	Saturated density (g·cm <sup>−3</sup> )	Permeability coefficient (10 <sup>–7</sup> cm·s <sup>–1</sup> )
S1-1	1.34	1.71	1.69
S1-2	1.28	1.67	2.36
S1-3	1.37	1.64	2.13
S2-1	1.23	1.58	1.23
S2-2	1.25	1.61	1.58
S2-3	1.27	1.72	1.19
S3-1	1.14	1.52	2.91
S3-2	1.1	1.49	5.54
S3-3	1.17	1.48	2.73

Table 3: Mechanical properties of SAP concrete materials

Group no.	Compressive strength (MPa)	Elasticity modulus (MPa)
S1	3.8	399
S2	5.8	922
S3	2.1	179

#### 5.2 Triaxial mechanical properties

Considering that buffer materials may be applied in environments with certain confining pressures, it is necessary to study the mechanical properties of SAP concrete under specific confining pressures and calculate the shear strength parameters  $(c, \varphi)$  of SAP concrete. In the triaxial tests, three confining pressures of 0.5, 1, and 1.5 MPa were selected. Note that before testing, it is necessary to fill all apparent pits on the specimen surface with silicone rubber



**Figure 17:** Stress–strain curves of SAP concrete materials under uniaxial conditions.

to prevent the confining pressure from damaging the heatshrink tubing.

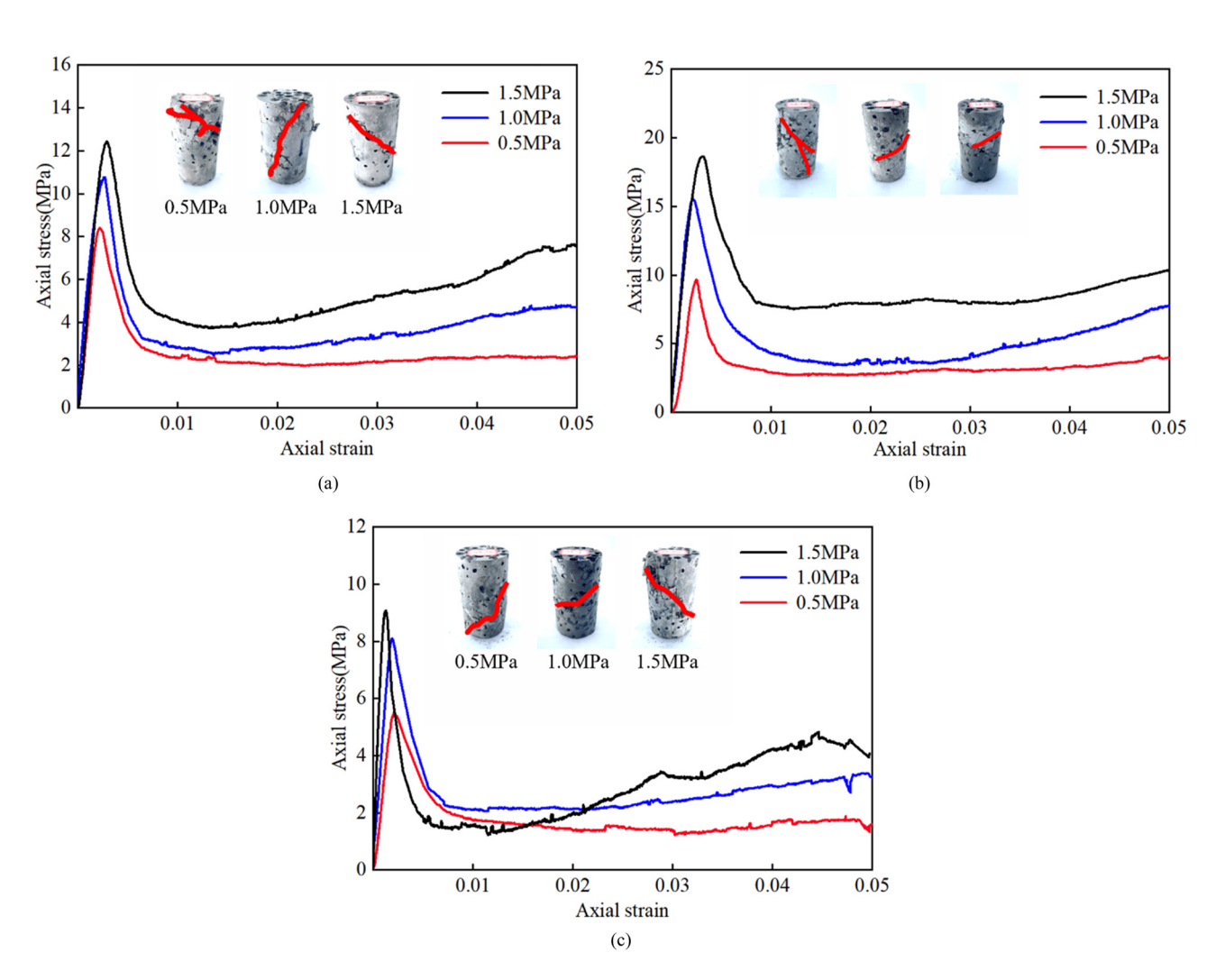


Figure 18: Triaxial test results of SAP concrete. (a) S1, (b) S2, and (c) S3.

Figure 18 shows the typical stress–strain curves of SAP concrete under different confining pressures, with shear failure predominating in the triaxial stress state. After experiencing the initial linear elastic segment, the stress rises linearly with strain until reaching the peak strength and then falls rapidly, after which the curve tends to be smooth.

Residual strength refers to the frictional stress on the shear surface after failure. Figure 19 displays the trends of peak strength and residual strength with changing confining pressure. It was found that both peak stress and residual strength are positively correlated with confining pressure. As the confining pressure increases, the peak stress and residual strength of SAP concrete significantly increase. This may be attributed to the confining pressure constraining the internal crack propagation and lateral expansion of the SAP concrete.

The shear strength parameters of SAP concrete can also be calculated based on the triaxial tests, as shown in Table 4. According to Coulomb's law, they can be calculated as follows:

$$\tau = c + \sigma \tan \varphi. \tag{2}$$

The calculations indicate that the friction angle of SAP concrete ranges between 40 and 50°, with cohesion values of 0.6–1.7 MPa. According to multiaxial mechanical tests on foam concrete [13,35–37], the friction angle of foam concrete is typically less than 30°. As measured by Liu et al. [36], foam concrete with a density of 600–800 kg·m<sup>-3</sup> and a uniaxial strength of 0.5–2.5 MPa has a friction angle between 15 and 24° [35], which is considerably lower than that of SAP concrete with comparable strength (S3). Generally, materials with a smaller friction angle have higher tensile strength

Table 4: Shear strength index

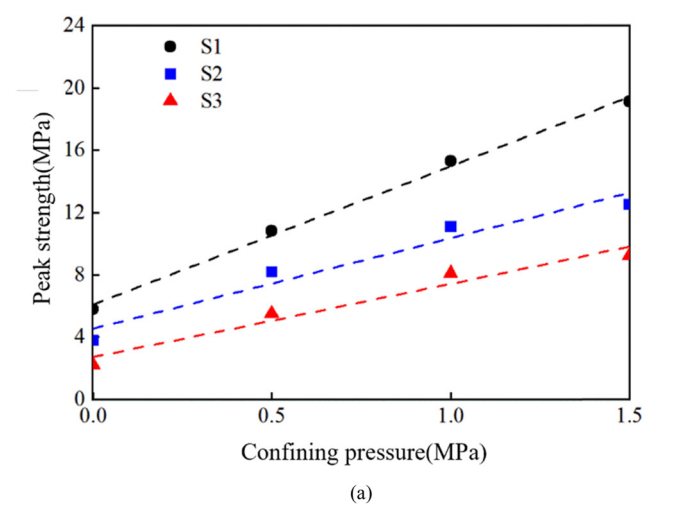
Group no.	Friction angle φ (°)	Cohesive <i>c</i> (MPa)
S1	44.0	1.30
S2	49.8	1.66
S3	43.3	0.65

and ductility, while those with a larger friction angle exhibit greater brittleness [38]. This also substantiates the higher brittleness of SAP concrete.

### 6 Characteristics of SAP concrete as a buffer material

Previously, some scholars [16,35] used foam concrete as an anti-seismic buffer material for tunnels and conducted triaxial compression tests on it. The stress–strain curves of foam concrete and SAP concrete under triaxial stress conditions are summarized in Figure 20, where dashed lines represent typical stress–strain curves and solid lines denote summary curves. Under triaxial conditions, SAP concrete still exhibits distinct brittle characteristics, rapidly declining after reaching peak strength due to fragmentation and losing most of its load-bearing capacity, while foam concrete demonstrates noticeable ductile characteristics, undergoing strain hardening after the elastic phase.

The brittleness index D is defined as the ratio of residual strength to peak strength and is used to quantify the brittleness of a material. A smaller brittleness index



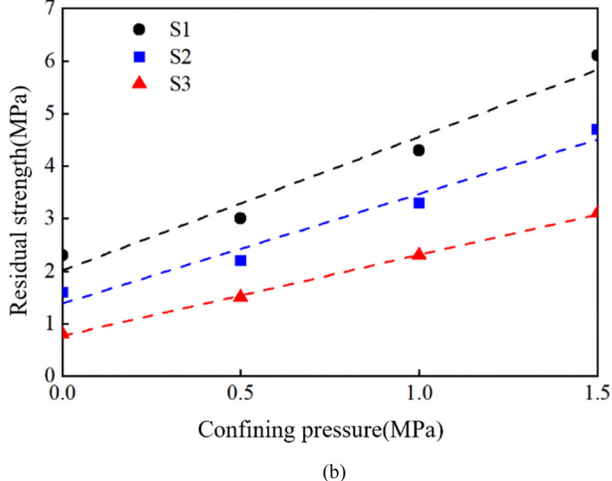
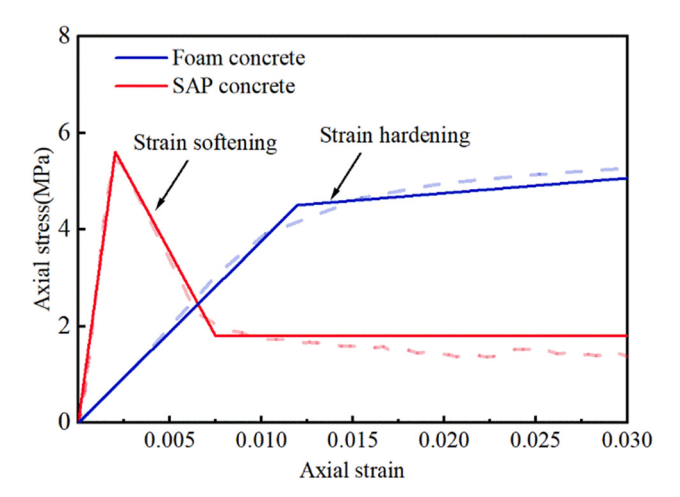


Figure 19: Peak and residual strength of SAP concrete at different surrounding pressures. (a) Peak strength and (b) residual strength.



**Figure 20:** Generalized graph of stress–strain curves of SAP concrete and foam concrete.

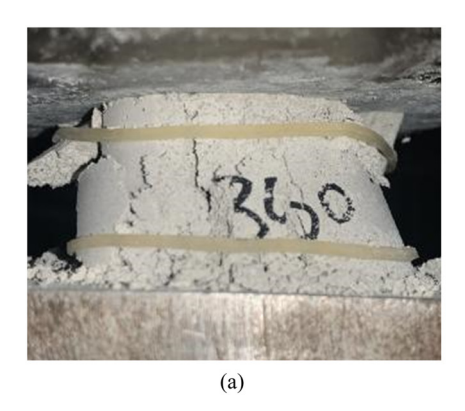
indicates greater brittleness of the material. For SAP concrete under uniaxial conditions or confining pressures lower than 1.5 MPa, the calculated brittleness index D typically ranges between 0.2 and 0.5. A review of related literature reveals that for foam concrete's stress—strain curves, the brittleness index D usually exceeds 0.5 and can even surpass 1 under confining pressures up to 1.5 MPa. This implies the occurrence of strain hardening, characterized by significant ductility.

The typical failure modes of foam concrete and SAP concrete are illustrated in Figure 21. Compared to foam concrete, SAP concrete fractures into smaller fragments after damage, while foam concrete demonstrates compaction of pores.

As a material with good ductility, foam concrete is often used in the soft surrounding rock areas of tunnels, offering yield support with its large deformation or serving as a seismic buffering material with excellent energy absorption capabilities in earthquake-prone areas. However, in fault zones, when severe stick-slip dislocations occur, the stress in foam concrete reaches yield strength, and the material undergoes strain hardening and pore compaction, increasing its strength. This makes it difficult for foam concrete to continue protecting the secondary lining. In contrast, SAP concrete buffer material exhibits distinct brittle characteristics. It rapidly fractures post-yield, creating large deformations to absorb the displacements caused by stick-slip dislocations. Moreover, it does not transfer large loads to the secondary lining, thereby offering better protection to the secondary lining.

Through the aforementioned experiments, the physical and mechanical properties of SAP concrete were studied, and the advantages of SAP concrete compared to other buffer materials were analyzed. Furthermore, it was found that under certain confining pressures, both the peak strength and residual strength of SAP concrete significantly increased, which is not conducive to the buffering effect of SAP concrete. Therefore, in design and construction, it is necessary to minimize the confining pressure on SAP concrete as much as possible, for instance, by installing the buffer material in a precast sectional manner at intervals.

To verify the feasibility of the intermittent arrangement of brittle buffer profiles for anti-dislocation, model tests were conducted. In these tests, foam gypsum was used to simulate the brittle buffer material, as shown in Figures 22 and 23. The tunnel structure remained intact without suffering severe damage, confirming the viability of brittle buffer materials for anti-dislocation. Additionally, larger cubic buffer profiles were prepared, measuring  $500 \text{ mm} \times 500 \text{ mm} \times 500 \text{ mm}$ , to confirm the feasibility of fabricating large-volume profiles. They simulated the destruction state of the original profiles during faulting, as depicted in Figure 24. Upon compressive failure, they rapidly lost load-bearing capacity, providing ample deformation space for the



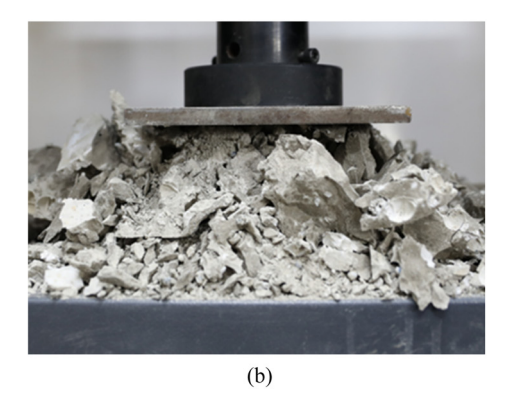


Figure 21: Comparison of typical failure patterns of foam concrete and SAP concrete. (a) Failure state of foam concrete and (b) failure state of sap concrete.

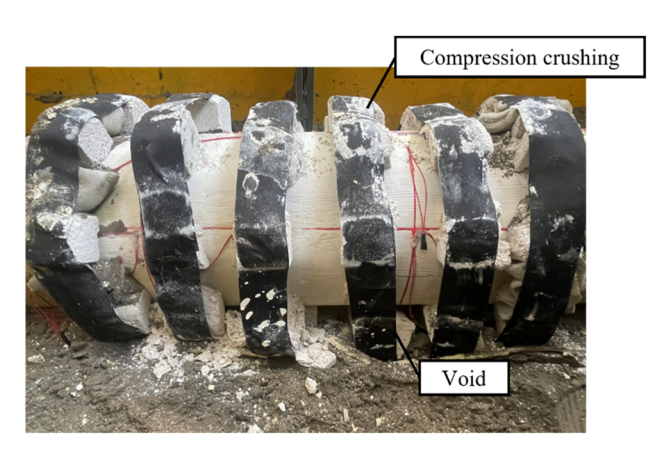
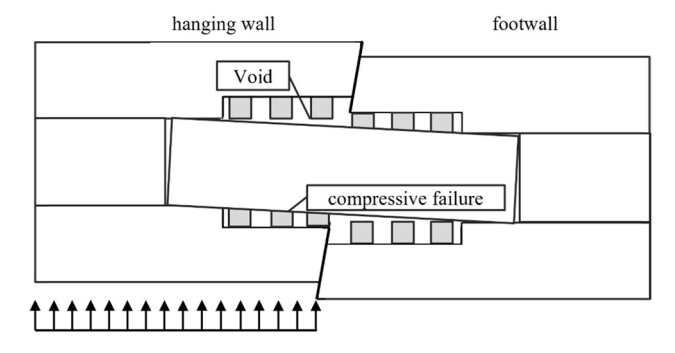


Figure 22: Model test results.

surrounding rock, confirming the feasibility of this material as a brittle buffer.

#### 7 Discussion

This study introduces a method for anti-dislocation using brittle buffer materials and develops corresponding brittle buffers, empirically demonstrating their feasibility and pioneering the application of SAP concrete materials in the field of tunnel engineering. The research systematically explored the physical and mechanical properties of SAP concrete, showcasing its potential to effectively mitigate the impact of fault dislocation on tunnel structures. A key discovery is the material's ability to rapidly fracture post-yield, providing substantial deformation space and thus alleviating the pressure on the secondary lining. This characteristic, along with the observed increase in strength under confining pressures, underscores the need for careful design considerations to fully exploit the material's benefits while reducing potential drawbacks. The comparison with foam concrete accentuates the superior



**Figure 23:** Schematic diagram of SAP concrete cushioning block to resist mis-fracture.



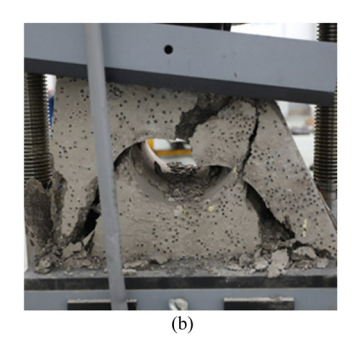


**Figure 24:** SAP concrete damage state. (a) Initial form and (b) after destruction.

brittleness of SAP concrete, advantageous for rapid stress relief. Finally, combining the strengths and weaknesses of SAP concrete, a method involving the intermittent arrangement of precast brittle buffer blocks for anti-dislocation is proposed, offering a novel direction for tunnel displacement prevention designs.

#### 8 Conclusions

- a) We developed a method for the pre-treatment of SAP aggregate using an alkaline solution. The pre-treated SAP aggregate exhibited a slow rate of water loss in the cement slurry, effectively preventing segregation bleeding and enhancing the strength of the cement slurry through slow dehydration during the later stages of solidification due to humidity differences.
- b) The uniformity of SAP concrete was assessed through section cutting, CT scanning, and sampling. The permeability coefficient of SAP concrete was determined to be in the order of 10<sup>-7</sup> cm·s<sup>-1</sup> through a soft wall permeability test, indicating slightly lower permeability compared to foam concrete of the same density.
- c) The prepared SAP concrete exhibited a strength range of 1–6 MPa. Compared to foam concrete, which showed noticeable strain hardening, SAP concrete demonstrated clear strain softening, indicating its brittle nature as opposed to the ductile behavior of foam concrete. The peak and residual strengths of SAP concrete were found to be significantly and positively correlated with the confining pressure, increasing notably as the confining pressure increased. This is likely due to the confining pressure limiting the expansion of microcracks and lateral displacement within the SAP concrete, thereby enhancing the material's overall load-bearing capacity.
- d) Utilizing the brittle characteristics of SAP concrete material, we applied it to tunnels affected by stick-slip

- dislocation. Its rapid loss of compressive capacity under stress provides substantial yielding capability, effectively buffering and protecting the lining from damage.
- e) Our study of the physical and mechanical properties of SAP concrete demonstrates its feasibility and characteristics as an anti-dislocation buffer layer for tunnels. As a novel type of anti-dislocation buffer material, SAP concrete has not yet been validated in actual tunnel engineering. Future research should focus on the mechanical properties of large-sized SAP concrete components, tunnel model tests of the SAP concrete buffer layer, and related numerical simulations to further understand and optimize its application.

**Acknowledgments:** The financial support from the National Key R&D Programs for Young Scientists (no. 2023YFB2390400), the **National** Natural Science Foundation of China (nos. 52379112, U21A20159, 52079133), Key Research Program of FSDI (2022KY56(ZDZX)-02), Key Research Program of the Ministry of Water Resources (SKS-2022103), Visiting Researcher Fund Program of State Key Laboratory of Water Resources Engineering and Management (Grant No. 2023SGG07), and the project of Key Laboratory of Water Grid Project and Regulation of Ministry of Water Resources (QTKS0034W23291) are sincerely acknowledged.

**Funding information:** The work is supported by National Key R&D Programs for Young Scientists (no. 2023YFB2390400), the National Natural Science Foundation of China (nos. U21A20159, 52079133, 52379112, 41902288), Key Research Program of FSDI (2022KY56(ZDZX)-02), Key Research Program of the Ministry of Water Resources (SKS-2022103), and Yunnan Major Science and Technology Special Program (202102AF080001).

Author contributions: All authors have accepted responsibility for the entire content of this manuscript and approved its submission.

**Conflict of interest:** The authors state no conflict of interest.

Data availability statement: The datasets generated and/ or analyzed during the current study are available from the corresponding author on reasonable request.

#### References

Uenishi, K. and S. Sakurai, Characteristic of the vertical seismic waves associated with the 1995 Hyogo-ken Nanbu (Kobe), Japan

- earthquake estimated from the failure of the Daikai underground station. Earthquake Engineering & Structural Dynamics, Vol. 29, No. 6, 2000, pp. 813-821.
- [2] Bray, J. D. Developing mitigation measures for the hazards associated with earthquake surface fault rupture. In Proc. workshop on seismic fault-induced failures—possible remedies for damage to urban facilities, University of Tokyo, Japan, 2001, 55-79.
- Gundes Bakir, P., G. De Roeck, G. Degrande, and K. K. F. Wong. Site [3] dependent response spectra and analysis of the characteristics of the strong ground motion due to the 1999 Duzce earthquake in Turkey. Engineering Structures, Vol. 29, No. 8, 2007, pp. 1939-1956.
- O'Rourke, T. D., S. H. Goh, C. O. Menkiti, and R. J. Mair. Highway tunnel performance during the 1999 Duzce earthquake. In Proceedings of the Fifteenth International Conference on Soil Mechanics and Geotechnical Engineering; 27-31 August 2001, 2, Istanbul, 1365-1368.
- Yang, H. W. and J. Beeson. The setback distance concept and 1999 Chi-Chi (Taiwan) earthquake. In Proceedings of the Fourth International Conference on Recent Advances in Geotechnical Earthquake Engineering and Soil Dynamics. CD-ROM, paper no. 10.56, Prakash, S., eds, University of Missouri-Rolla, San Diego, 2001.
- Kelson, K. I., K. H. Kang, W. D. Page, C. T. Lee, and L. S. Cluff. [6] Representative styles of deformation along the Chelungpu fault from the 1999 Chi-Chi (Taiwan) earthquake: Geomorphic characteristics and responses of man-made structures. Bulletin of the Seismological Society of America, Vol. 91, No. 5, 2001, pp. 930-952.
- [7] Wang, W. L., T. T. Wang, J. J. Su, C. H. Lin, C. R. Seng, and T. H. Huang. Assessment of damages in mountain tunnels due to the Taiwan Chi-Chi Earthquake. Tunnelling Underground Space Technol, Vol. 16, 2001, pp. 133-150.
- [8] Zhang, J., Z. Mei, and X. Quan. Failure characteristics and influencing factors of highway tunnels damage due to the earthquake. Disaster Advances, Vol. 6, 2013, pp. 142-150.
- [9] Pingliang, C., G. Ping, C. Junbo, and G. Wengi. The seismic damage mechanism of Daliang tunnel by fault dislocation during the 2022 Menyuan Ms6.9 earthquake based on unidirectional velocity pulse input. Engineering Failure Analysis, Vol. 145, 2023, id. 107047.
- Shahidi, A. R. and M. Vafaeian. Analysis of longitudinal profile of the tunnels in the active faulted zone and designing the flexible lining (for Koohrang-III tunnel). Tunnelling and Underground Space Technology, Vol. 20, No. 3, 2005, pp. 213-221.
- Guanxiong, Z., G. Ping, G. Xiangyu, L. Peisong, W. Qi, and D. Ti. An [11] anti-fault study of basalt fiber reinforced concrete in tunnels crossing a stick-slip fault. Soil Dynamics and Earthquake Engineering, Vol. 148, 2021, id. 106687.
- [12] Guangxin, Z., S. Qian, C. Zhen, W. Tiangiang, and M. Yalina. Investigating the deformation and failure mechanism of a submarine tunnel with flexible joints subjected to strike-slip faults. Journal of Marine Science and Engineering, Vol. 9, No. 12, 2021, id. 1412.
- [13] Wang, H., W. Z. Chen, X. J. Tan, H. M. Tian, and J. J. Cao. Development of a new type of foam concrete and its application on stability analysis of large-span soft rock tunnel. Journal of Central South University, Vol. 19, No. 11, 2012, pp. 3305-3310.
- [14] Wu, G., W. Chen, X. Tan, W. Zhao, S. Jia, H. Tian, et al. Performance of new type of foamed concrete in supporting tunnel in squeezing rock. International Journal of Geomechanics, Vol. 20, No. 2, 2020, id. 04019173.
- [15] Su, L., H. Liu, G. Yao, and J. Zhang. Experimental study on the closed-cell aluminum foam shock absorption layer of a high-speed railway tunnel. Soil Dynamics and Earthquake Engineering, Vol. 119, 2019, pp. 794-800.

- [16] Ma, S., W. Chen, and W. Zhao. Mechanical properties and associated seismic isolation effects of foamed concrete layer in rock tunnel. *Journal of Rock Mechanics and Geotechnical Engineering*, Vol. 11, No. 01, 2019, pp. 159–171.
- [17] Zhang, C., X. Tan, W. Chen, H. Tian, G. Wu, W. Zhao, et al. Investigation on the deformation and energy dissipation behaviors for foamed concrete filled polyethylene pipe under quasi-static axial compression. *Construction and Building Materials*, Vol. 370, 2023, id. 130557.
- [18] Zhang, C., X. Tan, H. Tian, and W. Chen. Lateral compression and energy absorption of foamed concrete-filled polyethylene circular pipe as yielding layer for high geo-stress soft rock tunnels. *International Journal of Mining Science and Technology*, Vol. 32, No. 5, 2022, pp. 1087–1096.
- [19] Mei, X., Q. Sheng, Z. Cui, M. Zhang, and D. Dias. Experimental investigation on the mechanical and damping properties of rubber-sand-concrete prepared with recycled waste tires for aseismic isolation layer. *Soil Dynamics and Earthquake Engineering*, Vol. 165, 2023, id. 107718.
- [20] Mei, X., Z. Cui, Q. Sheng, J. Zhou, and C. Li. Application of the improved POA-RF model in predicting the strength and energy absorption property of a novel aseismic rubber-concrete material. *Materials*, Vol. 16, No. 3, 2023, id. 1286.
- [21] Yang, Q., P. Geng, J. Wang, P. Chen, and C. He. Research of asphalt–cement materials used for shield tunnel backfill grouting and effect on anti-seismic performance of tunnels. *Construction and Building Materials*, Vol. 318, 2022, id. 125866.
- [22] Ramamurthy, K., E. K. Kunhanandan Nambiar, and G. Indu Siva Ranjani. A classification of studies on properties of foam concrete. *Cement and Concrete Composites*, Vol. 31, No. 6, 2009, pp. 388–396.
- [23] Kunhanandan Nambiar, E. K. and K. Ramamurthy. Influence of filler type on the properties of foam concrete. *Cement and Concrete Composites*, Vol. 28, No. 5, 2006, pp. 475–485.
- [24] Jones, M. R. and A. McCarthy. Heat of hydration in foamed concrete: Effect of mix constituents and plastic density. *Cement and Concrete Research*, Vol. 36, No. 6, 2006, pp. 1032–1041.
- [25] Lapyote, P., T. Pipat, and Y. H. Kim. Review of concrete with expanded polystyrene (EPS): Performance and environmental aspects. *Journal of Cleaner Production*, Vol. 366, 2022, id. 132919.
- [26] Haghi, A. K., M. Arabani, and H. Ahmadi. Applications of expanded polystyrene (EPS) beads and polyamide-66 in civil engineering, Part One: Lightweight polymeric concrete. *Composite Interfaces*, Vol. 13, No. 4, 2006, pp. 441–450.

- [27] Zohuriaan-Mehr, M. J., H. Omidian, S. Doroudiani, and K. Kabiri. Advances in non-hygienic applications of superabsorbent hydrogel materials. *Journal of Materials Science*, Vol. 45, No. 21, 2010, pp. 5711–5735.
- [28] Mignon, A., D. Snoeck, K. D'Halluin, L. Balcaen, F. Vanhaecke, P. Dubruel, et al. Alginate biopolymers: counteracting the impact of superabsorbent polymers on mortar strength. *Construction and Building Materials*, Vol. 110, 2016, pp. 169–174.
- [29] Askarian, R., A. Darbhanzi, and R. Ranjbar Karimi. Internal curing of concrete by superabsorbent polymer particles. *Iranian Journal of Science and Technology, Transactions of Civil Engineering*, Vol. 46, 2022, pp. 3979–3994.
- [30] Xu, F., X. Lin, and A. Zhou. Performance of internal curing materials in high-performance concrete: A review. Construction and Building Materials, Vol. 311, 2021, id. 125250.
- [31] Suryawanshi, N. T., C. B. Nayak, S. B. Thakare, and G. K. Kate. Optimization of self-cured high-strength concrete by experimental and grey Taguchi modelling. *Iranian Journal of Science and Technology*, *Transactions of Civil Engineering*, Vol. 46, No. 6, 2022, pp. 4313–4326.
- [32] Deng, Z., H. Cheng, Z. Wang, G. Zhu, and H. Zhong. Compressive behavior of the cellular concrete utilizing millimeter-size spherical saturated SAP under high strain-rate loading. *Construction and Building Materials*, Vol. 119, 2016, pp. 96–106.
- [33] Ren, J., Z. Deng, H. Cheng, L. Zhou, and X. Zheng. Numerical simulation of dynamic mechanical properties of porous concrete fabricated with the SAP. *Modelling, Measurement and Control B*, Vol. 86, No. 2, 2017, pp. 535–556.
- [34] Wang, F., J. Yang, H. Cheng, J. Wu, and X. Liang. Study on mechanism of desorption behavior of saturated superabsorbent polymers in concrete. ACI Materials Journal, Vol. 112, No. 3, 2015.
- [35] Zhao, W., W. Chen, and K. Zhao. Laboratory test on foamed concrete-rock joints in direct shear. *Construction and Building Materials*, Vol. 173, 2018, pp. 266–275.
- [36] Liu, M., Z. Liu, K. Wang, C. Ma, H. Zhang, and P. Zhuang. Strength and deformation performances of silt-based foamed concrete under triaxial shear loading. *Journal of Building Engineering*, Vol. 60, 2022, id. 105237.
- [37] Su, B., Z. Zhou, Z. Li, Z. Wang, and X. Shu. Experimental investigation on the mechanical behavior of foamed concrete under uniaxial and triaxial loading. *Construction and Building Materials*, Vol. 209, 2019, pp. 41–51.
- [38] Gu, J. and P. Chen. A failure criterion for isotropic materials based on Mohr's plane theory. *Mechanics Research Communications*, Vol. 87, 2018, pp. 1–6.